AIP | Applied Physics Letters

Mode interference and radiation leakage in a tapered parallel plate waveguide for terahertz waves

R. Mueckstein, M. Navarro-Cía, and O. Mitrofanov

Citation: Appl. Phys. Lett. **102**, 141103 (2013); doi: 10.1063/1.4800772
View online: http://dx.doi.org/10.1063/1.4800772
View Table of Contents: http://apl.aip.org/resource/1/APPLAB/v102/i14
Published by the American Institute of Physics.

Additional information on Appl. Phys. Lett.

Journal Homepage: http://apl.aip.org/
Journal Information: http://apl.aip.org/about/about_the_journal
Top downloads: http://apl.aip.org/features/most_downloaded
Information for Authors: http://apl.aip.org/authors

ADVERTISEMENT

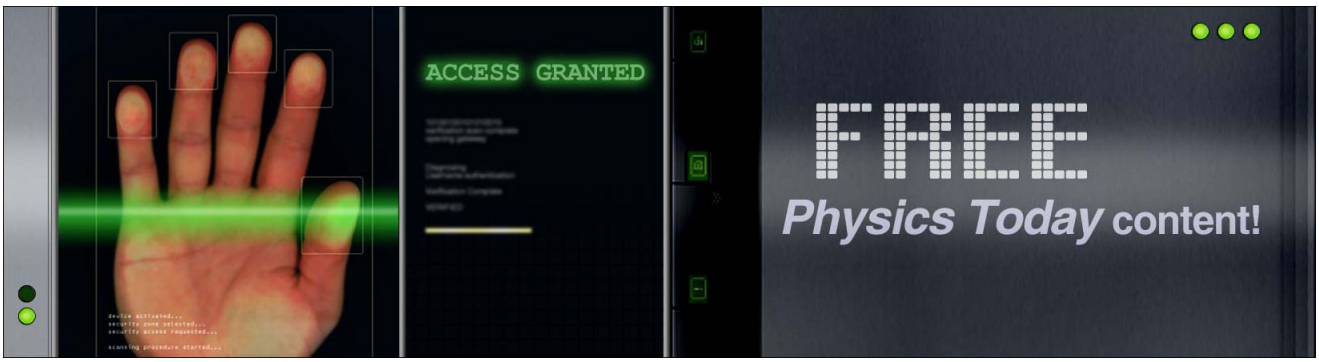

Downloaded 20 Jun 2013 to 144.82.107.87. This article is copyrighted as indicated in the abstract. Reuse of AIP content is subject to the terms at: http://apl.aip.org/about/rights_and_permissions

Mode interference and radiation leakage in a tapered parallel plate waveguide for terahertz waves

R. Mueckstein,[1,a)] M. Navarro-Cía,[1,2,b)] and O. Mitrofanov[1,c)]
[1]*Department of Electronic & Electrical Engineering, University College London, Torrington Place, London WC1E 7JE, United Kingdom*
[2]*Optical and Semiconductor Devices Group, Department of Electrical and Electronic Engineering, Imperial College London, London SW7 2BT, United Kingdom; Centre for Plasmonics and Metamaterials, Imperial College London, London SW7 2AZ, United Kingdom; and Centre for Terahertz Science and Engineering, Imperial College London, London SW7 2AZ, United Kingdom*

(Received 16 January 2013; accepted 25 March 2013; published online 9 April 2013)

To exploit tapered parallel plate waveguides for broadband terahertz (THz) spectroscopy, the impact of the waveguide geometry on transmission of terahertz pulses is investigated experimentally. We find that the approximation of single transverse electro-magnetic mode propagation is insufficient for describing the observed behavior. The TE_{02} mode plays a particularly important role. The mode composition, however, can be controlled by the gap between the waveguide plates, which affects the main loss mechanism, radiation leakage, and group velocity for the TE_{02} mode. Balancing the waveguide loss and coupling efficiencies results in an optimal gap for the tapered waveguide. © *2013 American Institute of Physics*. [http://dx.doi.org/10.1063/1.4800772]

Tapered parallel plate waveguides (PPWGs) have recently been proposed for confining terahertz (THz) pulses to sub-wavelength spatial dimensions with the aim of improving THz spectroscopy and imaging techniques.[1,2] THz pulse propagation without distortion is expected in the PPWG due to the formation of the dispersion-less transverse electro-magnetic (TEM) mode.[3] The assumption of single TEM mode propagation, however, may not hold true in some PPWG geometries. When the excitation does not properly match the TEM mode, higher order modes are likely to be excited. Also, yet less evident, the finite dimensions of the waveguide plates and the tapered configuration can lead to the formation of higher order modes due to reflections of the TEM mode at the plate edges. Interference of these modes and conversion of higher-order modes to the TEM-like mode causes pulse distortion in a tapered PPWG as it will be demonstrated below. The current understanding of energy transfer in the tapered PPWG based on the single TEM mode propagation, therefore, can lead to incorrect interpretation of spectroscopic features when higher-order modes are present.

Control of the mode composition in the PPWG can be achieved by adjusting the distance between the waveguide plates, which will be referred to as the gap in this paper. The gap size not only dictates the cut-off frequencies of higher order modes but also determines the weight of different loss mechanisms for each mode and controls the input and output coupling coefficients.[4–7] In this paper, we investigate propagation of THz pulses in a tapered PPWG and evaluate the dependence of transmission losses on the waveguide gap size with the aim of mitigating the effects of multimode propagation.

We discuss an important series of non-canonical transverse electric $TE_{0,n}$ modes, which have not been mentioned in the literature. The nomenclature of these modes is chosen by analogy with the mode notation for rectangular waveguides with artificial boundaries.[8] These modes develop due to the superposition of reflections of the TEM mode experienced at the edges of the PPWG. We underline that the TE_{02} mode in particular plays a critical role in modifying the waveform of the transmitted THz pulse and, thus, the spectrum at the output of the waveguide considered here.

We find that in waveguide configurations with gap sizes comparable to the THz wavelength, the main loss mechanism is radiation leakage into free-space. Radiation leakage allows controlling the mode composition; however, it has not been discussed in detail for tapered PPWGs. Based on these findings and the examination of the input and output coupling efficiencies, we determine an optimal gap size for maximum energy transfer through the tapered PPWG.

We consider a tapered PPWG made of aluminum with geometrical parameters designed for guiding THz pulses over a distance of several centimeters (Fig. 1(a)): the input width $w_{in} = 4.4$ mm was chosen to be significantly larger than the input THz beam diameter to make input coupling independent of this parameter. The output width of $w_{out} = 1$ mm is intentionally larger than the wavelength to allow better out-coupling into free-space. The waveguide length of 29.4 mm was chosen to form the taper angle θ recommended in the literature.[2] The guiding surfaces were polished with sub-micrometer grit lapping paper to minimize scattering losses during propagation.[9] A surface roughness of 30 nm was determined with an atomic force microscope by measuring the average deviation from the mean height in several regions along the waveguide. Both plates of the PPWG are mounted on separate translation stages, which allow controlling the gap size p between the plates.

To investigate THz pulse propagation through the waveguide, we use a near-field THz time-domain spectroscopy system[10] with an integrated sub-wavelength aperture near-field THz probe[11] at the PPWG output. The use of the

[a)]Electronic mail: r.mueckstein@ee.ucl.ac.uk
[b)]Electronic mail: m.navarro@imperial.ac.uk
[c)]Electronic mail: o.mitrofanov@ucl.ac.uk

 © 2013 American Institute of Physics

Downloaded 20 Jun 2013 to 144.82.107.87. This article is copyrighted as indicated in the abstract. Reuse of AIP content is subject to the terms at: http://apl.aip.org/about/rights_and_permissions

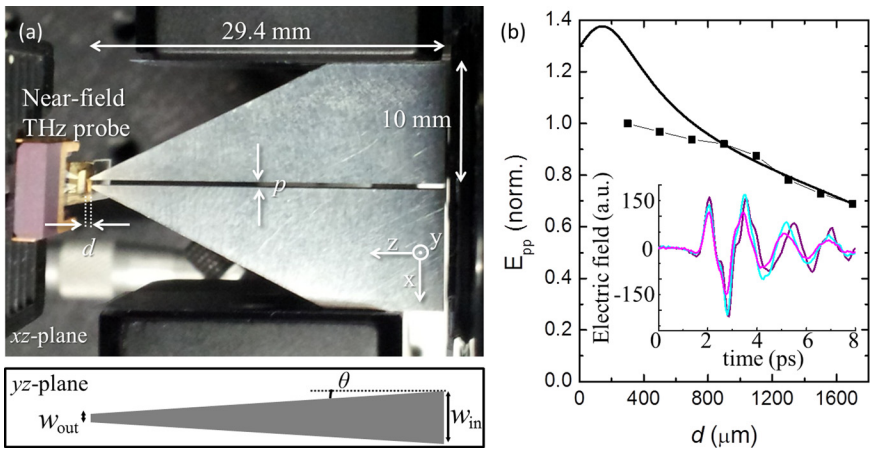

FIG. 1. (a) *xz*-plane view of the experimental setup (top); a schematic diagram of the guiding surface (*yz*-plane view, bottom); (b) Simulated (solid line) and measured (squares) peak to peak electric field amplitude of the THz pulse at the PPWG output as a function of the distance *d*. Inset: detected THz waveforms for $d = 300$ (purple), $d = 900$ (cyan), and $d = 1700\,\mu$m (magenta).

near-field probe for detection of transmitted pulses directly at the output avoids potential pulse distortion due to focusing elements, such as lenses and parabolic mirrors. The probe contains a gold surface with a 50 μm square aperture positioned perpendicular to the waveguide axis. The photoconductive antenna of the probe is oriented to detect the electric field component E_x.

For generation of THz pulses, we use a 1 mm thick ZnTe non-linear crystal to rectify 100 fs optical pulses ($\lambda = 800$ nm and $P = 400$ mW). The crystal is mounted on a 500 μm thick GaAs plate to block the optical beam from entering the waveguide. The GaAs plate/ZnTe crystal assembly is positioned 500 μm away from the PPWG input. The optical beam is aligned to the center of the input gap at $x = y = 0\,\mu$m. The THz beam diameter at the PPWG input was estimated by moving the excitation point along the *x*-direction ($y = 0\,\mu$m) from $x = -500\,\mu$m to $x = +500\,\mu$m (in steps of 50 μm) and recording the THz pulse amplitude. This procedure is equivalent to the convolution of the incident beam with the input aperture of the waveguide and allows estimating the FWHM of the Gaussian beam to be $\sim 500\,\mu$m $\pm 100\,\mu$m.

In order to ensure that the near-field probe presence does not affect the detected THz pulse waveforms, the distance *d* between the probe and the PPWG output was varied from 300 μm to 1700 μm while the gap between the plates was kept at 500 μm. We did not notice significant changes in the detected waveforms (inset in Fig. 1(b)). It indicates that the presence of the probe does not have a significant impact on the measured results. As expected, we observed a drop in the amplitude when moving the detector away from the PPWG output. The electric field decreases by 30% due to energy divergence outside the waveguide. Numerical simulations confirmed these observations. In all experiments presented below, the THz detector is kept at 500 μm away from the PPWG output. At this distance, experimental errors in the relative position of the probe and the PPWG cause negligible variation of the detected signal amplitude, allowing a comparative study of pulse transmission for different waveguide configurations.

Despite the dispersion-free behavior of the TEM mode, experimental results show that the THz pulses experience distortion due to propagation in the waveguide. Detected waveforms depend on the gap size, which was varied from $p = 0\,\mu$m (the closed waveguide configuration) up to $p = 3000\,\mu$m. Figure 2(a) shows waveforms for three different gap sizes representative of three distinctive regimes. For small gaps ($p = 100\,\mu$m), the pulse exhibits the shortest waveform: the main pulse is followed by only small oscillations up to $t = 10$ ps. For $p = 500\,\mu$m, the waveform is

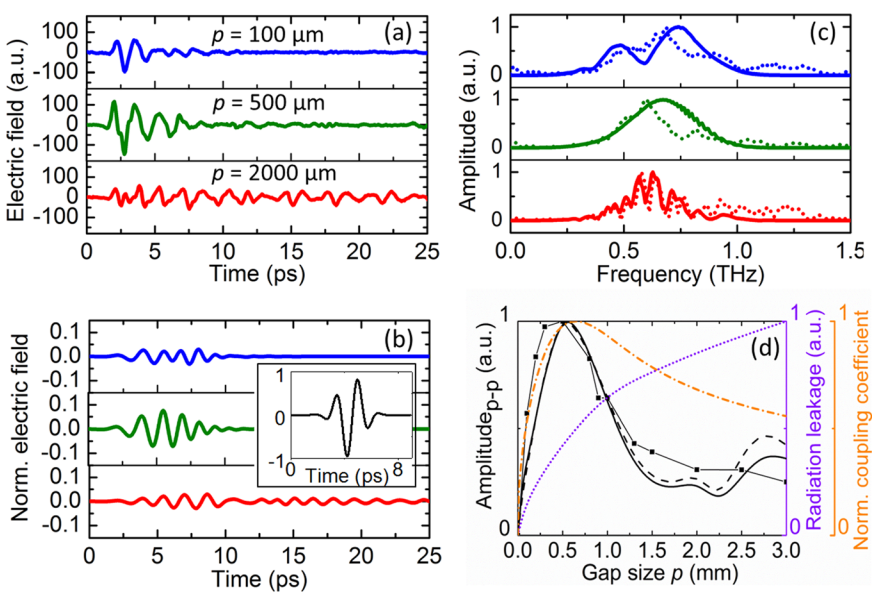

FIG. 2. (a) Measured THz pulse waveforms for different gap sizes *p*. (b) Simulated waveforms for the configurations shown in (a) and the THz input pulse (Inset); the electric fields are normalized to the input pulse. (b) Simulated waveforms for the configurations shown in (a) and the simulated THz input pulse (Inset); the waveforms are normalized to the amplitude of the input pulse waveform. (c) Measured (dotted lines) and simulated spectra (solid lines) of the waveforms in (a) and (b). (d) Experimentally measured (black squares) and simulated (solid and dashed lines) peak-to-peak amplitudes of the THz pulse as a function of the gap size. The solid and the dashed lines correspond to the simulation with and without the detector present. Coupling coefficient (orange dash-dotted line) and an estimation of the radiation leakage (violet dotted line) as a function of the gap size.

Downloaded 20 Jun 2013 to 144.82.107.87. This article is copyrighted as indicated in the abstract. Reuse of AIP content is subject to the terms at: http://apl.aip.org/about/rights_and_permissions

noticeably longer (lasting up to $t = 8$ ps) and it is followed by a series of small oscillations up to 16 ps. Finally, for $p = 2000\ \mu$m, a main pulse is not visible anymore and oscillations of comparable amplitude are present up to the end of our scan ($t = 25$ ps).

Spectra of these waveforms (displayed in Fig. 2(c)) show a very different and, at a first glance, puzzling behavior. For the gap size of 100 μm, the spectrum exhibits a dip at about 0.6 THz, which would not be expected for a waveform with minimal dispersion. For $p = 500\ \mu$m, the spectrum is unexpectedly slightly smoother, but still has some structure with a minimum at 0.75 THz. Finally, an elaborate periodic structure is present in the spectrum for $p = 2000\ \mu$m. The periodic oscillations suggest the presence of mode beating for this configuration.

In order to shed more light on these results, the experimental system is modeled numerically with the commercial software CST MICROWAVE STUDIO™ using the finite integration time domain formulation. As a source, a Gaussian beam is defined at 0.69 THz with the following parameters to be consistent with the experimental configuration: the minimum beam waist is 280 μm (i.e., Rayleigh length of 566 μm) and the source center is placed at 500 μm from the PPWG input. The temporal waveform (inset in Fig. 2(b)) is described by a Gaussian envelope (pulse spectrum ~0.2–1 THz, FWHM ~2 ps).

A non-uniform discretization hexahedral mesh was used to map the geometry accurately. The maximum mesh step in the simulation box is 42 μm, whereas the cubic grid within the gap has been defined as 10 μm × 20 μm × 33 μm. The symmetry of the problem allowed for introducing electric and magnetic walls in the *yz* and *xz* planes (as defined in Fig. 1(a)), respectively, to reduce computation effort. Perfectly matched layers are defined in all simulation boundaries unless stated otherwise. The PPWG has been modeled with the bulk conductivity of aluminum $\sigma_{Al} = 3.56 \times 10^7$ S/m.

Simulations of the THz pulse transmission show three regimes as observed in the experiments (Fig. 2(b)). To understand the origins of waveform distortion, the output pulses are compared to the input pulse (Fig. 2(b) inset). The waveform for $p = 100\ \mu$m is composed of two consecutive pulses with waveforms similar to the input pulse. This waveform indicates propagation of two modes with different modal group delay: the fundamental TEM and a higher-order mode. It will be explained later using the simulated spatial electric field distribution that this mode is TE_{02}. This mode exhibits two half-cycles of the electric field in the *y*-direction with its maximum at the PPWG center and a constant field distribution in the *x*-direction. The output pulse spectrum (Fig. 2(c)) shows a dip at around 0.6 THz, corresponding to destructive interference of the two modes, in agreement with the experimental data. The waveform for $p = 500\ \mu$m also includes these two modes. However, they are in phase, appearing like a single continuous pulse with an envelope extending from 2 to 10 ps. The spectrum, as a result, shows a Gaussian-like shape without a noticeable effect of interference (Fig. 2(c)). Finally, for $p = 2000\ \mu$m, repeating oscillations occur throughout the whole temporal span, as it is observed in the experiment, indicating that the output pulse is transmitted by several modes. The corresponding spectrum displays periodic modulation, in good agreement with the experimental spectrum.

In order to prove the multimode nature of the output waveforms even for $p = 100\ \mu$m, we examine the numerically computed electric-field distribution inside the PPWG. We plotted the distribution in the *yz*-plane for three time delays: t_1, t_2, and t_3 ($t_2 = t_1 + 10$ ps, $t_3 = t_1 + 30$ ps) in Fig. 3. At the latest time t_3, there are unquestionably two different modes: the left one is uniform in the *y*-direction and can be assigned to the TEM mode. This is not only because of the spatial field distribution but also because of its modal group velocity, which is the highest among all modes. The TEM nature of this mode is clearly confirmed in the top panel of Fig. 3(b) where the *xy*-plane view of the E_x component is displayed for a specific time t_4. This time corresponds to the moment when the peak of the TEM mode reaches the imaging plane. The second mode arrives delayed with respect to the first mode (t_5) and it has characteristic side-lobes near the waveguide edges. The side-lobes are clearly displayed in the *yz*-plane at t_3, and for a later time t_5, at the waveguide output in the *xy*-plane (the bottom right panel). The field distribution inside the waveguide is constant along the *x*-axis, indicating that this mode distribution corresponds to the TE_{02} mode. Finally, behind the TE_{02} mode, traces of the TE_{04} mode can be seen for t_1 and t_2. This mode appears behind the other two modes because of its slower group velocity.

It is straightforward to distinguish the TEM and the TE_{02} modes at the time delay t_3 because they have propagated long enough to be spatially separated due to their different modal group velocities. However, at earlier times t_2 and t_1, for example, the TEM and TE_{02} modes overlap temporally, and the scenario is not so simple. Because of the mode interference, one can find certain times (t_1) when the TEM mode and the central lobe of the TE_{02} mode are out of phase. In this situation, these modes interfere destructively at the waveguide center and constructively at the edges, leading to the enhanced electric field near the waveguide edges, similarly to the effect discussed in Ref. 12. In our case, however, this distribution is clearly attributed to the interference of the TEM and TE_{02} modes rather than to the formation of plasmon modes.

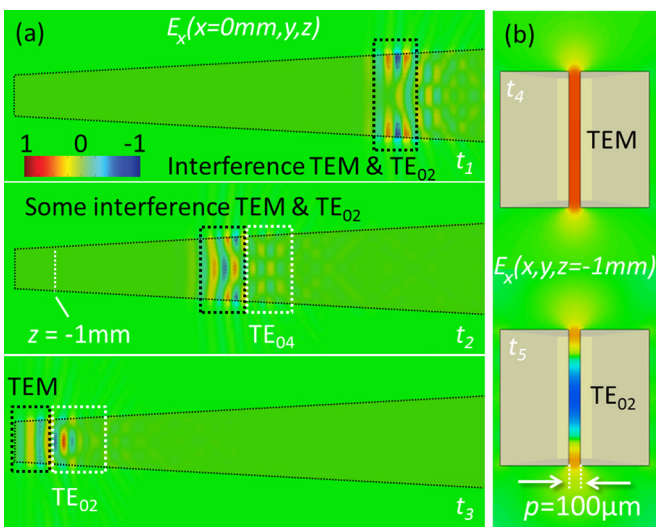

FIG. 3. (a) *yz* cross sectional view of the electric field $E_x(x = 0, y, z)$ for t_1, t_2, and t_3; (b) *xy* front view of the electric field E_x (x, y, $z = -1$ mm) close to the PPWG output for t_4 (top) and a later time t_5 (bottom).

Downloaded 20 Jun 2013 to 144.82.107.87. This article is copyrighted as indicated in the abstract. Reuse of AIP content is subject to the terms at: http://apl.aip.org/about/rights_and_permissions

We note that this multimode propagation is important even for a tapered PPWG with sub-wavelength output cross-sectional dimensions.[13] Although the TE_{02} mode runs into the cut-off ($f_{c,TE0,n} = cn/2w$,[14] where c is the free-space velocity), it nevertheless can have an important role in the formation of the PPWG output wave. Let us assume a starting point in the PPWG where both the TEM mode and the TE_{02} mode can propagate. For the sake of simplicity, all other modes are in cut-off. As the width of the waveguide is reduced, the side lobes of the TE_{02} leak out of the waveguide and convert into free-space radiation. Meanwhile, in the center of the waveguide, the central lobe converts into the TEM-like field distribution because it is the only field distribution allowed by the geometry. This TEM-like mode arrives later than the genuine TEM mode because of its initially different modal group velocity, i.e., TE_{02} group velocity. Hence, although the field distribution at the end of the waveguide appears as a single TEM mode, its origin involves the propagation of two separate modes.

The results in Fig. 2 show that the relative weight of the propagating modes can be controlled by the gap between the plates of the tapered PPWG. In order to optimize the waveguide for THz spectroscopic applications, it is, therefore, essential to understand how the gap size affects attenuation for each mode. The impact of different loss mechanisms is explained in Fig. 2(d), where the peak-to-peak amplitude of the THz pulse is plotted as a function of the gap size. One can see a strong increase in the amplitude up to a gap size of about 500 μm. Beginning from that point, the signal decreases and drops down to only 25% of its maximum value at a gap size of 3000 μm. This behavior is confirmed by computing the peak-to-peak amplitude numerically (solid black line).

The function shown in Fig. 2(d) can be clearly divided into two regions, corresponding to the gap size smaller and larger than 500 μm, which appears to be the optimal gap size for maximum energy transfer through the PPWG presented in this work. For gap sizes below approximately 500 μm, the energy transfer is primarily governed by the coupling coefficient of the waveguide. For comparison, we plot the coupling efficiency for a Gaussian beam (FWHM = 520 μm) and the TEM mode using the overlap integral[15] (dashed-dotted line). For gap sizes above 500 μm, energy transfer is not limited by the input coupling anymore and radiation leakage at the waveguide edges is the dominant effect. Since the PPWG plates are separated further from each other, the electric field is spatially less confined between the plates and it is, therefore, more likely to leak out through the open boundaries. The stronger leakage for wider gaps can also be explained by ordinary transmission line theory.[6] The PPWG impedance is $120\pi \times p/w$.[14] For small gaps ($p \ll w$), the impedance of the PPWG is much smaller than the one of free space. It prevents the energy leakage. When widening the gap size, the PPWG impedance gets closer to the free space impedance and reduces reflections at the PPWG edge. For a configuration where p is similar to w or even greater ($p \geq w$), the impact of the metallic plates on the propagating wave decreases and the waveguide impedance approaches the value of free-space for $p \gg w$.

The radiation leakage is also estimated numerically. Due to computation constraints, the leakage is evaluated by the integral: $\int_{t_0}^{t_f} \oiint_S |E(x,y,z,t)| dsdt$ where t_0 and t_f account for the times the THz signal enters and exits the PPWG, respectively, and S is the surface parallel to the waveguide edge with a width 400 μm wider than the respective gap size and a distance 100 μm away from the edges. The integral value is plotted in Fig. 2(d) as a violet curve. It confirms the expected trend towards higher radiation losses for wider gaps.

In summary, we investigate the impact of the gap size on transmission of THz pulses with the aim to exploit the tapered PPWG geometry for broadband terahertz spectroscopy. We find that the approximation of single TEM mode propagation is insufficient. Higher order modes are likely to be excited in the input coupling process given the mismatch between any free-space propagating beam and the fundamental TEM mode. This is especially relevant for a point source excitation as it is used in this work. Although the problem can be mitigated, for instance, by collimating the beam, this may not prevent the excitation of higher order modes within the tapered waveguide. In non-adiabatically tapered configurations, the reflections of the TEM mode at the PPWG boundary can result in the excitation of the $TE_{0,n}$ mode during propagation. We illustrate the case of the TE_{02} mode interference with the TEM mode and its effect on the waveform and spectrum of the transmitted pulse, even for geometries tapered to sub-wavelength size. The multimode interference effect can be mitigated by controlling the gap between the waveguide plates. The gap affects radiation leakage and group velocity for the higher-order modes. Modes with energy distribution close to the PPWG edges are more likely to be affected by this. Control of the gap also allows dispersion tuning in a practical THz spectroscopy system. An optimal gap size is found by balancing the loss and the input and output coupling efficiencies for the tapered PPWG.

This work was supported by the Royal Society [Grant No. UF080745] and Engineering and Physical Sciences Research Council [Grant No. EP/G033870/1]. Miguel Navarro-Cía was supported by the Imperial College Junior Research Fellowship.

[1]J. Liu, R. Mendis, D. M. Mittleman, and N. Sakoda, Appl. Phys. Lett. **100**, 031101 (2012).
[2]H. Zhan, R. Mendis, and D. M. Mittleman, J. Opt. Soc. Am. B **28**, 558 (2011).
[3]R. Mendis and D. Grischkowsky, Opt. Lett. **26**, 846 (2001).
[4]R. Mendis and D. M. Mittleman, J. Opt. Soc. Am. B **26**, A6 (2009).
[5]S.-H. Kim, E. S. Lee, Y. B. Ji, and T.-I. Jeon, Opt. Express **18**, 1289 (2010).
[6]K. Iwaszczuk, A. Andryieuski, A. Lavrinenko, Z.-C. Zhang, and P. U. Jepsen, Opt. Express **20**, 8344 (2012).
[7]M. Mbonye, R. Mendis, and D. M. Mittleman, Appl. Phys. Lett. **100**, 111120 (2012).
[8]M. Beruete, M. Navarro-Cía, and M. Sorolla Ayza, IEEE Trans. Microwave Theory Tech. **59**, 2180 (2011).
[9]M. Wächter, M. Nagel, and H. Kurz, Appl. Phys. Lett. **90**, 061111 (2007).
[10]O. Mitrofanov, T. Tan, P. R. Mark, B. Bowden, and J. A. Harrington, Appl. Phys. Lett. **94**, 171104 (2009).
[11]O. Mitrofanov, M. Lee, J. W. P. Hsu, I. Brener, R. Harel, J. F. Federici, J. D. Wynn, L. N. Pfeiffer, and K. W. West, IEEE J. Sel. Top. Quantum Electron. **7**, 600 (2001).
[12]J. Liu, R. Mendis, and D. M. Mittleman, Appl. Phys. Lett. **98**, 231113 (2011).
[13]N. Klein, P. Lahl, U. Poppe, F. Kadlec, and P. Kuzel, J. Appl. Phys. **98**, 014910 (2005).
[14]S. Ramo, J. R. Whinnery, and T. Van Duzer, *Fields and Waves in Communications Electronics* (John Wiley & Sons, Inc., Hoboken, NJ, 1994).
[15]G. Gallot, S. P. Jamison, R. W. McGowan, and D. Grischkowsky, J. Opt. Soc. Am. B **17**, 851 (2000).

Downloaded 20 Jun 2013 to 144.82.107.87. This article is copyrighted as indicated in the abstract. Reuse of AIP content is subject to the terms at: http://apl.aip.org/about/rights_and_permissions